RSC Sustainability

ROYAL SOCIETY OF CHEMISTRY

PAPER

View Article Online
View Journal | View Issue

Cite this: *RSC Sustainability*, 2025, **3**, 5580

Synergistic effect between *Anemone coronaria* and *Quercus robur* leaf extracts on mild steel corrosion in HCl 1 M solution: electrochemical and computational study

Sofia Kerouad, *[a] Youssef El-Gheryby,[bc] Issam Forsal,[a] Mohammed-Amine Edaala,[b] Loubna Kabiri,[a] Mohamed Mbarki[d] and Latifa Bouissane[ef]

The leaves of *Anemone coronaria* (AC) and *Quercus robur* (QR) were evaluated as ecological corrosion inhibitors for mild steel (MS) in 1 M HCl. Individual extracts (AC and QR) and a mixture of the two were tested at concentrations ranging from 0.1 to 0.5 g L^{-1} to investigate potential synergistic effects. The corrosion inhibition performance was assessed using potentiodynamic polarization (PDP) and electrochemical impedance spectroscopy (EIS). The results showed that corrosion resistance increased with inhibitor concentration, with individual efficiencies of 93.66% (AC) and 92% (QR), while the mixture achieved a maximum inhibition efficiency of 95%, indicating a synergistic effect. Fourier-transform infrared (FT-IR) spectroscopy revealed characteristic functional groups within the extracts, while scanning electron microscopy (SEM) confirmed the formation of a protective barrier on the steel surface. The adsorption process followed the Langmuir isotherm, and thermodynamic analysis revealed a spontaneous, mixed physisorption–chemisorption mechanism. DFT calculations revealed a strong interaction between the inhibitor molecules and the mild steel surface, characterized by a low energy gap (ΔE), supporting excellent anticorrosion performance at the molecular level. These findings demonstrate that the combined use of AC and QR extracts represents a novel, eco-friendly approach to corrosion inhibition, offering high efficiency, biodegradability, and minimal environmental impact.

Received 9th September 2025
Accepted 15th October 2025

DOI: 10.1039/d5su00738k

rsc.li/rscsus

Sustainability spotlight

Corrosion of mild steel in acidic environments is a major industrial problem that leads to material degradation, economic losses, and environmental concerns. Conventional corrosion inhibitors, often synthetic and toxic, pose risks to human health and ecosystems. In this work, we present a sustainable alternative by using eco-friendly extracts from *Anemone coronaria* and *Quercus robur*. Electrochemical experiments and density functional theory (DFT) confirm high inhibition efficiency (95%) and strong molecular interactions with steel surfaces. By reducing reliance on hazardous chemicals and promoting renewable natural resources, this research advances safer industrial practices and contributes directly to UN Sustainable Development Goals 9 (Industry, Innovation and Infrastructure), 12 (Responsible Consumption and Production), and 13 (Climate Action).

1. Introduction

The degradation of metallic materials represents a widespread challenge in numerous industrial sectors. Steel, widely used thanks to its favorable properties, cost-effectiveness and high strength, is particularly vulnerable to corrosion in many applications. Also, industries often rely on acidic environments for operations such as cleaning, oil well acidification, and chemical pickling of steels.[1,2] However, these acidic environments induce physicochemical changes in metal surfaces, leading to material deterioration and causing significant environmental and health concerns.[3] The corrosion of mild steel in acidic environments is an electrochemical process involving both anodic and cathodic reactions. The anodic reaction is characterized by the

[a]*Laboratory of Engineering and Applied Technologies, School of Technology, Beni Mellal, Morocco. E-mail: sofia.kerouad@usms.ac.ma*

[b]*Laboratoire de Chimie Analytique et Moléculaire, Faculté Polydisciplinaire de Safi, Université Cadi Ayyad, Sidi Bouzid, B.P. 4162, Safi 46000, Morocco*

[c]*Aix Marseille Université, CNRS, LCE, Bâtiment Villemin BP 80, 13545 Cedex 4 Aix-en-Provence, France*

[d]*Engineering in Chemistry and Physics of Matter Laboratory, Faculty of Science and Technologies, Sultan Moulay Slimane University, PB: 523, Beni Mellal, Morocco*

[e]*Molecular Chemistry, Materials and Catalysis Laboratory, Faculty of Sciences and Technologies, Sultan Moulay Slimane University, BP 523, 23000 Beni-Mellal, Morocco*

[f]*Chemicals Process and Applied Materials Team, Polydisciplinary Faculty, Sultan Moulay Slimane University, BP 523, Beni-Mellal, 23000, Morocco*

dissolution of iron into Fe^{2+} ions, while the cathodic reaction is mainly the reduction of hydrogen ions to form hydrogen gas. In hydrochloric acid solutions, chloride ions play a critical role by penetrating the oxide film and accelerating the dissolution process, which results in a higher corrosion rate of steel.[4–6]

To mitigate such degradation, numerous inorganic and organic inhibitors have been developed. Inorganic inhibitors, including chromates, phosphates, and silicates, have been widely employed, but their use is increasingly restricted due to their toxicity and adverse environmental impact.[7,8] Similarly, several synthetic organic inhibitors containing N, S, or O atoms have shown high efficiencies in acidic media.[9,10] However, their high cost, non-biodegradability, and potential carcinogenic risks limit their practical applications. These limitations have shifted research efforts toward the exploration of plant-derived extracts as green corrosion inhibitors, since they can effectively reduce steel corrosion while minimizing ecological risks.[11] Such natural inhibitors are biodegradable, non-toxic, cost-effective, and fully consistent with the principles of green chemistry.[12]

Several researchers have reported the successful use of natural plant extracts for the corrosion inhibition of mild steel in various acidic media.[13–21] The leaf extract of Eucalyptus acted as a mixed-type inhibitor in 0.5 M H_2SO_4 and 0.5 M H_3PO_4 solutions, showing higher efficiency in sulfuric acid, reaching up to 91% at a concentration of 0.4 mol L^{-1}.[22] Hyssopus officinalis (hyssop) leaf extract exhibited good inhibition in 0.5 M HCl for both mild steel and zinc alloy, achieving efficiencies up to 80%, primarily through physical adsorption.[23] Furthermore, Salix (willow) leaf extract acted as a mixed-type inhibitor in 0.5 M HCl and 0.5 M HNO_3, with higher efficiency in nitric acid (~90%).[24] These studies demonstrate that plant extracts, which are rich in bioactive compounds such as flavonoids, tannins, and phenolic acids, can effectively adsorb onto steel surfaces and form protective films, thereby significantly reducing corrosion in acidic environments.

Anemone coronaria and *Quercus robur* were selected as potential eco-friendly corrosion inhibitors due to their high content of bioactive compounds and their ecological and medicinal significance. *Anemone coronaria* is rich in flavonoids, alkaloids, and phenolic compounds, which are well-known for their strong antioxidant properties and ability to adsorb onto metallic surfaces, thereby facilitating the formation of protective films that inhibit steel corrosion.[25] *Quercus robur*, commonly known as English oak, contains abundant tannins, polyphenols, and flavonoids, compounds that can effectively interact with iron substrates through electron donation and π–π interactions, leading to the retardation of both anodic and cathodic reactions.[26] Moreover, the combination of these two plant extracts has not been extensively studied, and their complementary phytochemical profiles suggest a potential synergistic effect, which could enhance the overall inhibition efficiency compared to individual extracts. The selection of AC and QR is therefore based not only on their rich phytochemistry but also on their potential to provide a sustainable, biodegradable, and non-toxic alternative to conventional chemical inhibitors, aligning with the principles of green chemistry and current environmental regulations.

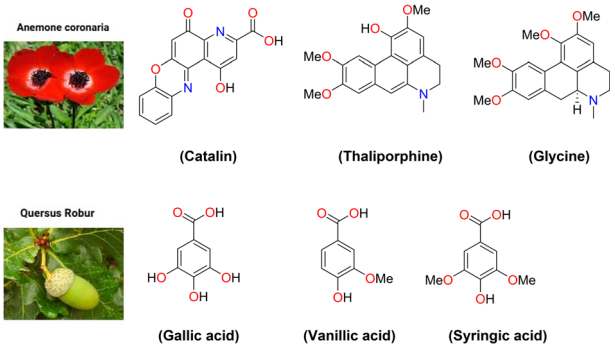

Fig. 1 Molecular structures of the major phytoconstituents present in the *Anemone coronaria* and *Quercus robur*.

Based on previous studies,[27,28] representative molecules were selected for DFT analysis, including catalin, thaliporphine, and glaucine found in *Anemone coronaria*, and gallic acid, vanillic acid, and syringic acid found in *Quercus robur* (Fig. 1). These molecules were chosen due to their reported bioactivity, making them suitable candidates for exploring the molecular-level mechanisms of corrosion inhibition.

Building on this rationale, the present study evaluates the corrosion-inhibiting performance of extracts from *Anemone coronaria* and *Quercus robur*, both individually and as a combined mixture, acting as eco-friendly inhibitors against mild steel degradation in 1 M HCl. The novelty of this work lies in the simultaneous investigation of two plant extracts and their representative bioactive molecules, supported by DFT calculations, electrochemical techniques (PDP and EIS), SEM, and FT-IR analyses, to elucidate inhibition mechanisms at both molecular and surface levels. This approach not only provides insight into the adsorption behavior of natural inhibitors but also highlights their key advantages, including low toxicity, biodegradability, cost-effectiveness, and minimal environmental impact.

2. Experimental

2.1. Materials

The corrosion tests were performed on a mild steel sample corresponding to AISI 1018 grade and composed of Fe (96.2%), C (0.164%), Mn (0.710%), Si (0.260%), S (0.001%), and P (0.005%). Before each experiment, the steel surface was mechanically polished with successive grades of SiC abrasive papers (#400–2000) in order to obtain a smooth and uniform surface. The samples were then thoroughly rinsed with distilled water, degreased with ethanol, and finally air-dried. The 1 M HCl solution was then employed, and its molarity was verified through acid–base titration using a sodium hydroxide (NaOH) solution.

2.2. Extracts preparation

Leaves of *Anemone coronaria* were harvested from Boufekrane, Morocco, while those of *Quercus robur* were collected from the Beni-Mellal region. The collected plant material was thoroughly

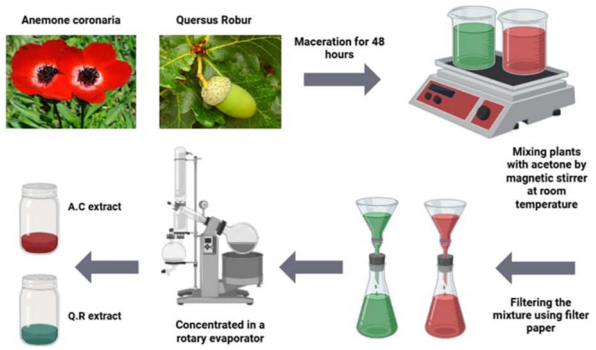

Fig. 2 Flowchart of leaves extraction procedure.

washed with distilled water and shade-dried for 10 days at ambient temperature. Subsequently, 15 g of the dried leaf powder were extracted with 250 mL of acetone under continuous stirring for 48 h. The mixture was filtered, and the solvent was removed by rotary evaporation, yielding a concentrated crude extract (Fig. 2).

A stock solution was prepared by dissolving the crude extract in 1 M HCl, and working solutions with concentrations of 0.5, 0.4, 0.3, 0.2, and 0.1 g L^{-1} were obtained by appropriate dilution. These concentrations were selected to investigate the effect of inhibitor dosage on the corrosion protection efficiency.

2.3. Electrochemical experiment

Electrochemical measurements were carried out using a controlled potentiostat (OrigaStat) equipped with OrigaMaster analysis software. A conventional three-electrode corrosion cell was employed, consisting of a platinum counter electrode (surface area 1 cm^2), a $Hg/Hg_2Cl_2/KCl_{sat}$ (SCE) reference electrode, and a mild steel (MS) working electrode. Prior to measurements, the MS was immersed in the test solution under open circuit potential (OCP) conditions for 0.5 h to ensure stabilization and determine the equilibrium potential (E_{ocp}).

EIS data was acquired at frequencies ranging from 1 kHz to 100 mHz with a 10 mV peak-to-peak sinusoidal potential. PDP techniques were used to capture current–potential curves within a potential variation between −750 mV and −100 mV at a scan rate of 1 mV s^{-1}.

2.4. Surface analysis

FT-IR spectroscopy was employed to identify the bioactive phytoconstituents of *Anemone coronaria* and *Quercus robur* and to characterize the functional groups and bonding patterns present on their surfaces. FTIR analysis was conducted using a JASCO FT/IR-4600 spectrometer equipped with an ATR accessory. Spectra were recorded over the 4000–600 cm^{-1} range at a resolution of 4 cm^{-1}, accumulating 16 scans.

The metal specimens were polished, degreased with acetone, dried, and subsequently immersed in 1 M HCl solution for 24 h at 293 K in the absence and presence of the plant extracts. Surface morphology was then analyzed utilizing a scanning electron microscope (SEM, JSM-IT10) at a magnification of 32× to evaluate the effects of corrosion and the possible development of protective film.

2.5. Density functional theory (DFT)

Density functional theory (DFT) is increasingly employed to describe molecular properties, elucidate mechanisms of action, and predict the efficiency of corrosion inhibitors. In this study, DFT calculations were performed using Materials Studio 2023 (ref. 29) with the DMol³ module. The geometry of the selected corrosion inhibitor molecules was optimized, and their electronic properties were calculated using the generalized gradient approximation (GGA) with the Perdew–Burke–Ernzerhof (PBE)[30] functional and a double numerical plus polarization (DNP) basis set. The self-consistent field (SCF) convergence criterion was set to 0.00005 Ha. HOMO–LUMO energies and electrostatic potential (ESP) surface maps were obtained to analyze the electronic distribution and identify potential reactive sites.[31,32]

3. Results and discussion

3.1. FTIR

Fig. 3 presents the FT-IR spectra of *Anemone coronaria* (A) and *Quercus robur* (B) extracts. Both extracts are rich in bioactive substances including flavonoids, polyphenols, alkaloids, and tannins, which provide a significant contribution to the inhibition of corrosion. The spectra reveal the existence of different functional groups: carbonyl, hydroxyl, aromatic rings, amine and ether. These polar groups are known to enhance the affinity of organic molecules for metal surfaces by facilitating molecular interactions and surface coverage. Their presence suggests that the extracts' molecules can effectively attach to the steel substrate, creating a barrier that protects it from the aggressive acidic medium.[33–35]

3.2. Effect of concentration

3.2.1. PDP study. PDP curves of MS in 1 M HCl at 293 K, obtained in the absence and in the presence of varying doses of the three tested inhibitors, are shown in Fig. 4. Inhibited and uninhibited solutions present similar polarization curves, suggesting that the extracts have no influence on the corrosion process of the steel.[36] As the inhibitors' concentrations rises, the curves shift toward lower current densities, reflecting a decline in corrosion rate. Additionally, the (+) shift observed in the E_{corr} shows that the extracts reduce steel dissolution and inhibit

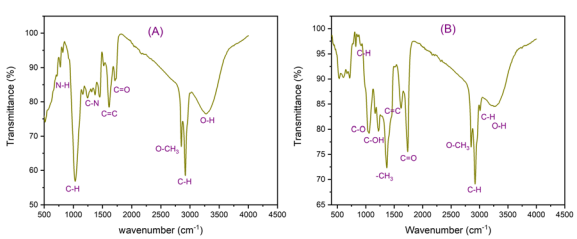

Fig. 3 FTIR spectra of (A) *Anemone coronaria* and (B) *Quercus robur* extracts.

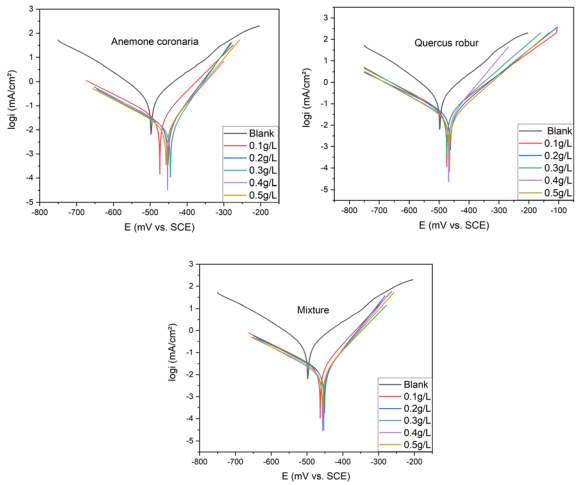

Fig. 4 PDP curves of the MS in HCl medium with varying concentrations of AC, QR and mixture.

hydrogen evolution in the acidic medium.[37] The parallel cathodic branches imply that the hydrogen evolution reaction mechanism remains activation-controlled.[38]

Table 1 summarizes the electrochemical data obtained from the linear regions of the anodic and cathodic Tafel plots. The IEPDP, % was calculated using eqn (1):[39]

$$IE_{PDP}\% = \frac{I_{corr} - I_{corr}(inh)}{I_{corr}} \times 100 \quad (1)$$

where I_{corr} and I_{corr}(inh) are the corrosion current densities in the absence and presence of the inhibitor.

The literature reports that an inhibitor can be classified as anodic or cathodic if its corrosion potential (E_{corr}) shifts by more than ±85 mV. In this work, the E_{corr} displacement observed for the combined extract lies between −70.73 mV and −82.85 mV, which indicates that the inhibition mechanism is of mixed type.[40,41] As shown in Table 1, increasing the inhibitor concentration significantly reduced the corrosion current density (I_{corr}), from 229.76 μA cm^{-2} in the blank solution to 20.4, 43.1, and 20.2 μA cm^{-2} for *Anemone coronaria*, *Quercus robur*, and their mixture, respectively, with the highest inhibition efficiency (96.12%) obtained for the combined extract, reflecting the restricted access of the electrolyte to the steel surface.[42] In parallel, both anodic (β_a) and cathodic (β_c) Tafel slopes decreased with increasing inhibitor concentration. This behavior suggests that the adsorption of inhibitor molecules onto the steel surface blocks active sites for electrochemical reactions, while allowing electron transfer during hydrogen evolution.[43] Overall, these results demonstrate that the mixture acts as an efficient mixed-type inhibitor, significantly reducing the corrosion rate.

3.2.2. EIS study. Electrochemical impedance spectroscopy (EIS) is a widely used technique for evaluating the corrosion inhibition performance of green inhibitors at the steel–HCl interface. This approach provides essential information on the insulating and barrier properties of the protective layer formed by the inhibitors, while maintaining the advantage of being non-destructive owing to its operation at low applied potentials.

The characteristic capacitive loop observed in the Nyquist diagram reflects both the electrochemical susceptibility of MS to corrosion and the ability of the plant extracts to mitigate this process by forming a resistive film at the metal–solution interface. Fig. 5 displays the Nyquist diagrams of MS in HCl medium with different concentrations of inhibitors. All spectra exhibit capacitive semicircles, confirming that the corrosion mechanism is controlled by a charge-transfer process.[44] The slight distortion of the semicircles is attributed to the surface heterogeneity of the electrode.[45] The similarity in the overall shape of the plots, regardless of the inhibitor concentration, indicates that the fundamental corrosion mechanism remains unchanged, revealing that the corrosion process is not influenced by the presence of inhibitors. However, the progressive enlargement of the capacitive loops with increasing inhibitor concentration reflects a significant increase in charge-transfer resistance. This behavior is associated with the formation of a protective film at the steel/HCl interface, which acts as

Table 1 Polarization data for MS in the presence and absence of inhibitors

	C	E_{corr} (mV)	I_{corr} (μA cm^{-2})	β_a (mV)	$-\beta_c$ (mV)	IE_{pdp}%
HCL	1 M	−535.823	229.76	175.357	142.955	
AC	0.5 g L^{-1}	−456.755	13.4	55.6	126.5	94.16
	0.4g L^{-1}	−452.966	15.9	50	128.7	93.07
	0.3 g L^{-1}	−445.097	16.9	54.5	147.4	92.64
	0.2 g L^{-1}	−479.520	18.0	62.6	97.9	92.16
	0.1 g L^{-1}	−483.120	20.4	70.7	150.2	91.12
QR	0.5 g L^{-1}	−465.072	20.6	83.2	128.8	91.03
	0.4g L^{-1}	−468.018	22.9	60.8	128.2	90.03
	0.3 g L^{-1}	−474.285	33.7	83.1	126.6	85.33
	0.2 g L^{-1}	−462.353	35.7	88.5	149.5	84.46
	0.1 g L^{-1}	−473.917	43.1	99.8	136.2	81.24
Mixture	0.5 g L^{-1}	−465.085	8.9	53.1	100.7	96.12
	0.4g L^{-1}	−456.641	13.4	55.6	126.5	94.16
	0.3 g L^{-1}	−452.966	15.9	58	128.2	93.07
	0.2 g L^{-1}	−451.466	18.5	56	137.7	91.94
	0.1 g L^{-1}	−463.110	20.2	57.7	125.8	91.20

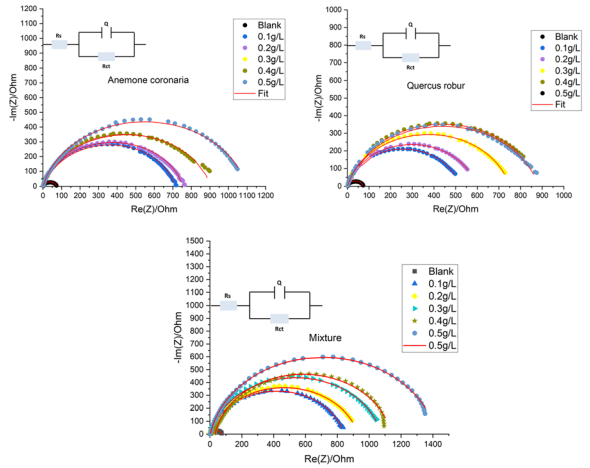

Fig. 5 Nyquist plots of the MS in the presence and the absence of various amounts of AC, QR and mixture in 1 M HCl at 293 K.

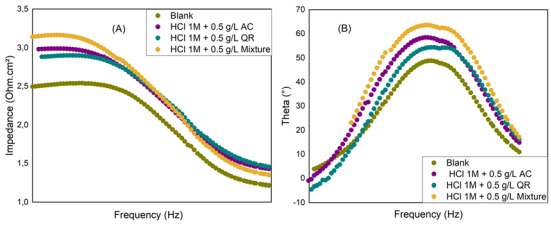

Fig. 6 (A) Bode impedance and (B) Bode theta spectra of the MS in the presence and the absence of 0.5 g L^{-1} of AC, QR and mixture in 1 M HCl at 293 K.

a barrier limiting the access of aggressive species to the metal surface and thereby enhancing corrosion resistance.[46]

The corresponding electrochemical parameters (R_s, R_{ct} and C_{dl}) are summarized in Table 2.

The Bode impedance spectra presented in Fig. 6A show that the addition of inhibitors increases the impedance modulus, implying that they effectively retard the corrosion rate of mild steel in the acidic medium. The phase angle values shown in the Bode theta plot (Fig. 6B) are lower than 90°, indicating non-ideal behavior that reflects the presence of inhomogeneities in the system. Moreover, the phase angle is observed to increase with the addition of inhibitors. This increase can be attributed to the reduction of the capacitive behavior at the mild steel surface, resulting from its lower dissolution rate in the presence of the extracts.[47,48]

The Randles equivalent circuit is commonly used to model electrochemical interfaces, assuming an ideal capacitive behavior of the electrode surface. However, even after careful cleaning, MS surfaces remain heterogeneous due to microstructural variations and surface roughness, leading to deviations from this ideal behavior. To account for this, the double-layer capacitance (C_{dl}) was replaced by a Constant Phase Element (CPE), which more accurately represents non-ideal interfaces by combining capacitive and resistive characteristics. The use of a CPE reflects the heterogeneous nature of the system and provides a better fit to impedance data. Accordingly, the EIS results were simulated using an electrical circuit model composed of the solution resistance (R_s) in series with a parallel branch of the charge-transfer resistance (R_{ct}) and the CPE, as illustrated in Fig. 7.[49,50] The inhibition efficiency (IE%) was calculated using eqn (2):[51]

$$(\mathrm{IE}_{\mathrm{EIS}}\%) = \frac{R_{ct} - R_{ct}^{\circ}}{R_{ct}} \times 100 \quad (2)$$

where R_{ct} and R_{ct}° represent the charge transfer resistance in the presence and absence of the inhibitor.

Table 2 summarizes the EIS parameters, including R_s, R_{ct}, CPE and n, which provide insight into deviations from ideal capacitive behavior. The exponent n, ranging from 0 to 1, characterizes this deviation and is often associated with surface heterogeneity and roughness. When n approaches 0, the Constant Phase Element (CPE) behaves predominantly as a resistor, whereas values close to 1 indicate behavior similar to an ideal capacitor.

Table 2 EIS data for MS in the presence and the absence of inhibitors

	C	R_s (Ω cm^2)	R_{ct} (Ω cm^2)	C_{dl} (μF cm^{-2})	n	$\mathrm{IE}_{\mathrm{EIS}}$%	F_{max}
HCl	1 M	2.377	70.68	96.26	0.90		2×10^{-5}
AC	0.5 g L^{-1}	1.163	1050	51.42	0.85	93.66	3×10^{-6}
	0.4 g L^{-1}	0.656	932.6	50.64	0.83	92.42	3.37×10^{-6}
	0.3 g L^{-1}	0.464	887.2	54.66	0.85	92.03	3.28×10^{-6}
	0.2 g L^{-1}	0.125	744.2	57.66	0.85	90.50	3.7×10^{-6}
	0.1 g L^{-1}	0.115	706.6	49.95	0.86	89.99	4.5×10^{-6}
QR	0.5 g L^{-1}	0.151	882.7	56.85	0.83	92	3.17×10^{-6}
	0.4 g L^{-1}	0.118	819.1	54.75	0.85	91.37	3.29×10^{-6}
	0.3 g L^{-1}	0.102	749.1	55.5	0.85	90.56	3.82×10^{-6}
	0.2 g L^{-1}	0.213	593.4	70.75	0.85	88.08	3.8×10^{-6}
	0.1 g L^{-1}	0.872	516.6	64.07	0.83	86.31	4.8×10^{-6}
Mixture	0.5 g L^{-1}	2.898	1416	55.06	0.85	95 $\pm$ 0.21	2.04×10^{-6}
	0.4 g L^{-1}	3.504	1108	55.87	0.85	93.62 $\pm$ 0.44	2.57×10^{-6}
	0.3 g L^{-1}	0.023	1076	38.67	0.86	93.43 $\pm$ 0.16	3.82×10^{-6}
	0.2 g L^{-1}	2.69	931.5	52.05	0.84	92.41 $\pm$ 0.39%	3.28×10^{-6}
	0.1 g L^{-1}	0.737	842.7	59.64	0.83	91.61 $\pm$ 0.47%	3.16×10^{-6}

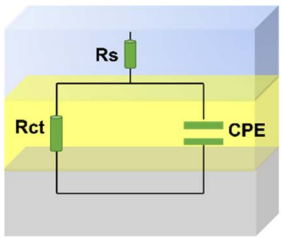

Fig. 7 Equivalent circuit model used to fit EIS data for MS in 1 M HCl.

The data reveals that the n ranges from 0.83 to 0.86, indicating that the corrosion behavior of MS deviates from the ideal response predicted by the equivalent circuit in the presence of inhibitors.[52] The decrease in n values suggests a reduction in the double-layer capacitance and further confirms that the CPE does not behave as a purely capacitive element.[53] Such deviations from ideal behavior are expected, as the dissolution process in the HCl solution produces a heterogeneous surface on the MS. Relative to the blank solution, the charge-transfer resistance (R_{ct}) exhibited a marked increase upon the addition of inhibitors and further increased with higher inhibitor concentrations. This trend reflects the formation of a protective adsorption layer on the steel surface, which limits charge transfer and improves corrosion resistance.[54] As shown in Table 2, increasing the inhibitor concentration led to a corresponding increase in both R_{ct} and inhibition efficiency (IE%), achieving maximum values of 92% for *Quercus robur*, 93.66% for *Anemone coronaria*, and 95% for their mixture at 0.5 g L^{-1}. These results are in strong agreement with the findings from the PDP analysis, confirming the effectiveness of the combined extract in providing superior protection compared to the individual components.

3.3. SEM analysis

In this study, SEM analysis was performed to examine the surface morphology of MS after exposure to 1 M HCl for 6 h in the absence and presence of plant extracts. Fig. 8(a) displays the polished steel surface before immersion, showing a smooth and uniform appearance with no visible defects. In contrast, Fig. 8(b) illustrates the specimen immersed in uninhibited 1 M HCl, where severe surface degradation is evident, characterized by deep pits and irregularities resulting from intense corrosion attack.[55,56] However, the surface of the samples treated with *Quercus robur* Fig. 8(d) and *Anemone coronaria* Fig. 8(c) extracts exhibit a noticeable improvement, showing reduced roughness and fewer defects compared to the blank, which confirms the surface coverage by the inhibitors. Remarkably, the specimen treated with the mixture of both extracts Fig. 8(e) presents the smoothest morphology with minimal irregularities, suggesting the formation of a dense and protective adsorbed layer, demonstrating superior inhibition efficiency compared to the individual extracts.

3.4. Effect of temperature

The effect of temperature on the inhibition process is complex, as it impacts both the corrosion behavior of MS and the stability

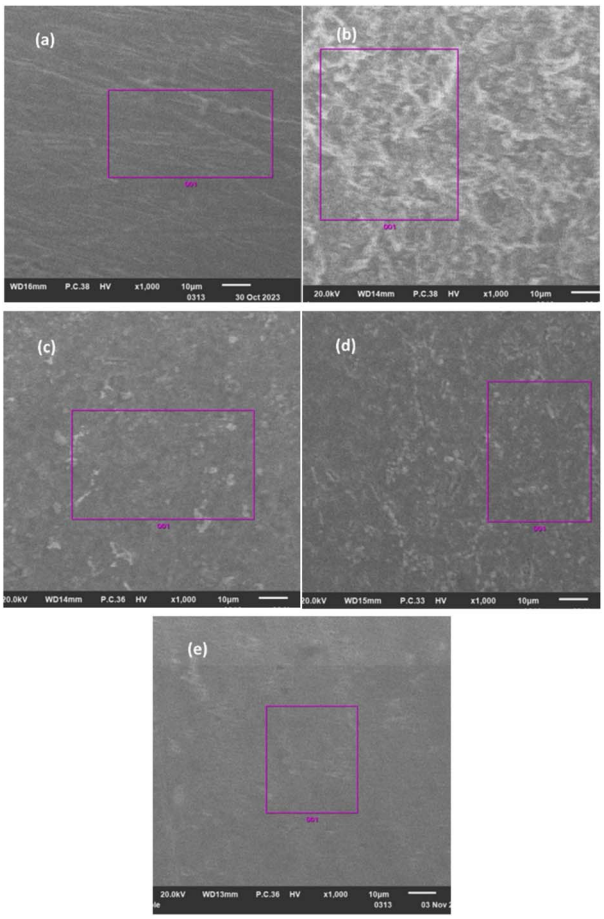

Fig. 8 SEM images of (a) polished steel (b) steel immersed in uninhibited 1 M HCl (c) steel immersed in 1 M HCl + *Anemone coronaria* (d) steel immersed in 1 M HCl + *Quercus robur* (e) steel immersed in 1 M HCl + mixture.

of the inhibitor. At elevated temperatures, accelerated desorption of inhibitor molecules may occur, leading to a decrease in protective performance.[57] In the present work, the influence of temperature was investigated in the range of 293 K to 323 K using the combined extract of *Anemone coronaria* and *Quercus robur*, which previously exhibited the highest inhibition efficiency (IE%). The tests were conducted at an inhibitor concentration of 0.5 g L^{-1}. The resulting current–potential (I–E) curves are illustrated in Fig. 9, and the corresponding

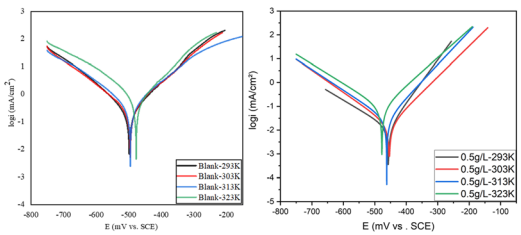

Fig. 9 The PDP plots of MS in 1 M HCl + 0.5 g L^{-1} of the mixture at different temperatures.

Table 3 Electrochemical parameters of MS in a 1 M HCl medium at 0.5 g L^{-1} of inhibitor

T (K)		I_{corr} (μA cm^{-2})	$-E_{corr}$ (mV)	β_a (mV)	$-\beta_c$ (mV)	IE_{pdp}%
293	Blank	229.76	487.88	86	107.7	—
303		286.97	494.72	96.8	115.5	—
313		398.52	494.54	110.2	121.4	—
323		635.62	476.51	93.1	114.1	—
293	Mixture	8.9	−465.08	53.1	100.7	96.12
303		17.2	−453.89	77	108.1	92.51
313		30.2	462.03	71.4	115.3	86.85
323		89.438	477.370	84.7	122.075	61.08

electrochemical parameters (E_{corr}, I_{corr}, and IE%) are summarized in Table 3.

The results show that I_{corr} increases with temperature in both inhibited and uninhibited media, indicating that corrosion becomes more severe at higher temperatures. However, the inhibition efficiency of the extract drops from 96.12% to 61.08%. This decrease can be attributed to the partial desorption of inhibitor molecules from the MS surface at elevated temperatures, which reduces the stability of the protective layer and enhances metal dissolution.[58] At higher temperatures, the steel surface becomes rougher, which hinders the adsorption of the inhibitor. The increase in temperature enhances molecular kinetic energy, leading to more vigorous interactions between the steel and the acidic medium, which accelerates metal dissolution. Additionally, it promotes greater dissociation of HCl, releasing more hydrogen ions, increasing acidity, and intensifying the corrosion process. This accelerated corrosion generates deeper pits and imperfections, further roughening the steel surface and allowing aggressive ions to penetrate more easily, thereby increasing the corrosion rate.[59,60]

To gain deeper insight into the corrosion inhibition mechanism, activation parameters including the activation energy (E_a), enthalpy of activation ($\Delta H°$), and entropy of activation ($\Delta S°$) were determined using the Arrhenius equation and transition state theory, as expressed in eqn (3) and (4). The Arrhenius and transition state plots are presented in Fig. 10A and B, respectively:

$$I_{corr} = Ae^{-E_a/RT} \quad (3)$$

$$I_{corr} = \frac{RT}{NH} e^{\Delta S°/R} e^{-\Delta H°/RT} \quad (4)$$

A is the frequency factor, R is the universal gas constant, N is Avogadro's and h is Planck's constant.

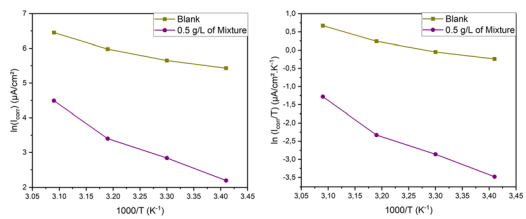

Fig. 10 (Left) Arrhenius plots and (Right) transition state plots of MS in 1 M HCl in the absence and presence of 0.5 g L^{-1} of inhibitor.

Table 4 The values of activation parameters for MS in 1 M HCl in the absence and presence of 0.5 g L^{-1} of inhibitor

Activation parameters	Blank	Mixture
E_a (KJ mol^{-1})	26.23	57.73
$\Delta H°$ (KJ mol^{-1})	23.36	55.17
$\Delta S°$ (KJ mol^{-1})	−120.29	−38.96

The calculated values of the activation parameters for MS in 1 M HCl, in the absence and presence of 0.5 g L^{-1} of the combined extract, are summarized in Table 4.

The results show that the activation energy increases significantly in the presence of the inhibitor, from 26.23 KJ mol^{-1} for the blank solution to 57.73 KJ mol^{-1} for the combined extract, suggesting that the inhibitor raises the energy barrier for the corrosion process. Such an increase in E_a is indicative of a physical adsorption (physisorption) mechanism, where the extract molecules form a protective layer that hinders mass and charge transfer at the MS surface.[61,62] Similarly, the enthalpy of activation ($\Delta H°$) rises from 23.36 to 55.17 KJ mol^{-1}, confirming the endothermic nature of the corrosion process and supporting the stabilization of the protective film at lower temperatures.[63] Moreover, the entropy of activation ($\Delta S°$) is negative in both cases, reflecting a decrease in disorder as the system transitions from reactants to the activated complex. These trends collectively support a predominantly physical adsorption mechanism, in which molecules interact with the steel surface through electrostatic forces and van der Waals interactions. The protective film limits mass and charge transfer, thus slowing down the corrosion process. Nevertheless, at higher temperatures, partial desorption of inhibitor molecules may occur, increasing the exposed metal surface and diminishing the inhibition efficiency. Overall, the combined extract stabilizes the transition state and forms a robust barrier, effectively mitigating MS corrosion in 1 M HCl.

3.5. Adsorption isotherm

Adsorption isotherms are essential tools for understanding the interaction mechanism between inhibitor molecules and the metal surface, providing insight into the nature, strength, and mode of adsorption.[64] In this study, the adsorption behavior of the inhibitor molecules on the MS surface in an acidic medium (1 M HCl) was thoroughly investigated to elucidate the

Table 5 Summary of adsorption isotherm models applied in corrosion inhibition study

Isotherm model	Linear equation	Eqn
Langmuir	$\frac{C_{inh}}{\theta} = \frac{1}{k_{ads}} + C_{inh}$	(5)
Freundlich	$\log\theta = \log k_{ads} + 1/n \log C_{inh}$	(6)
Flory–Huggins	$\log\left(\frac{\theta}{C_{inh}}\right) = \log k_{ads} + n \log(1-\theta)$	(7)
El-Awady	$\log\left(\frac{\theta}{1-\theta}\right) = y \log k_{ads} + y \log C_{inh}$	(8)

corrosion inhibition mechanism. The adsorption process plays a central role in corrosion protection, as the efficiency of an inhibitor is strongly correlated with its ability to form a stable and protective layer on the metal surface. A higher inhibition efficiency generally reflects an increased surface coverage (θ), indicating that the inhibitor molecules successfully replace water molecules and aggressive ions (Cl^-) at the steel/solution interface, thereby minimizing metal dissolution.[65]

To determine the most suitable adsorption model for describing this behavior, different isotherm models were examined, including Langmuir, Freundlich, El-Awady and Flory–Huggins, as presented in Table 5. Each of these models provides specific information on the adsorption mechanism: for instance, Langmuir assumes monolayer adsorption on a homogeneous surface, while Freundlich accounts for heterogeneous surface characteristics. By plotting the experimental data according to the linearized forms of these isotherms and calculating their correlation coefficients (R^2), the model that best fits the experimental results can be identified. This comparison not only confirms the adsorption mechanism but also allows the calculation of thermodynamic parameters, such as the adsorption equilibrium constant (K_{ads}) and the standard free energy of adsorption (ΔG°_{ads}), which provide further insight into whether the process follows physisorption, chemisorption, or a mixed mechanism.

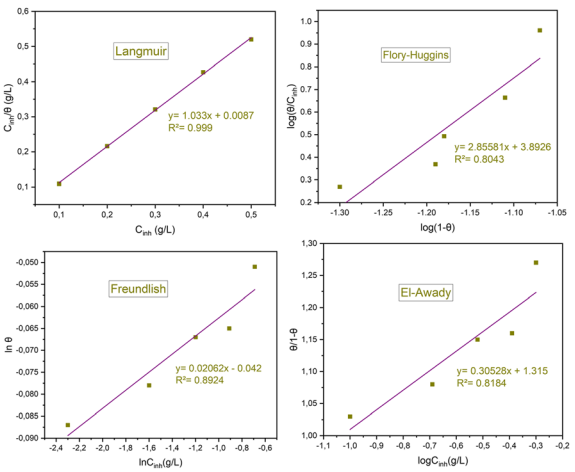

Fig. 11 Langmuir, Freundlich, Frumkin and Flory–Huggins isotherm models of mixture extract onto the MS.

The linear regression analysis (R^2) (Fig. 11) indicates that the Langmuir adsorption model provides the best fit for the EIS data obtained with the mixture extract in acidic medium, outperforming other models such as Freundlich, El-Awady and Flory–Huggins. The Langmuir plot displayed an excellent linear relationship with a correlation coefficient of $R^2 = 0.999$, which is very close to unity, confirming that the adsorption of inhibitor molecules on the MS surface follows the Langmuir model assumptions. According to this model, adsorption occurs at specific homogeneous sites on the metal surface, forming a uniform monolayer without significant interactions between adsorbed molecules.[66] This strong agreement suggests that the inhibitor molecules occupy the active sites of the steel surface in a one-to-one manner, creating a protective barrier that reduces metal dissolution. Furthermore, the equilibrium adsorption constant (K_{ads}) was derived from the intercept of the linear plot, and the standard free energy of adsorption (ΔG°_{ads}) was subsequently calculated following the eqn (9) and providing deeper insight into the spontaneity and nature of the adsorption process.

$$\left(\Delta G^{\circ}_{ads}\right) = -RT \ln(55.5\ K_{ads}) \quad (9)$$

Table 6 shows that the adsorption equilibrium constant (K_{ads}) for the mixed extract was found to be 114.94, indicating a strong affinity between the inhibitor molecules and the MS surface. Additionally, the negative value of ΔG°_{ads} (-21.34 KJ mol^{-1}) confirms that the adsorption process is spontaneous and thermodynamically favorable.[67] Additionally, it is generally accepted that values of ΔG°_{ads} more positive than -20 KJ mol^{-1} indicate physisorption, while those more negative than -40 KJ mol^{-1} correspond to chemisorption, however, when ΔG°_{ads} lies between these two limits, the adsorption is considered to involve a mixed mechanism of both physical and chemical interactions.[68,69] In the present case, the obtained value (-21.34 KJ mol^{-1}) falls slightly below -20 KJ mol^{-1}, suggesting that the adsorption process predominantly involves physisorption with a minor contribution from chemisorption. These interactions likely occur through electrostatic forces and possible weak chemical bonding between the active species of the inhibitor and the metal surface. Furthermore, the good agreement with the Langmuir isotherm highlights the strong surface coverage and effective interaction of the mixed extract with the steel substrate.

3.6. Theoretical calculation

Quantum chemical approaches, particularly density functional theory (DFT), are increasingly employed to investigate molecular characteristics, elucidate inhibition mechanisms, and estimate the efficiency of corrosion inhibitors. As a widely

Table 6 Summary of adsorption isotherm models applied in corrosion inhibition study

Isotherms	R^2	K_{ads}	Slope	ΔG°_{ads}
Langmuir	0.999	114.94	1.033	-21.34

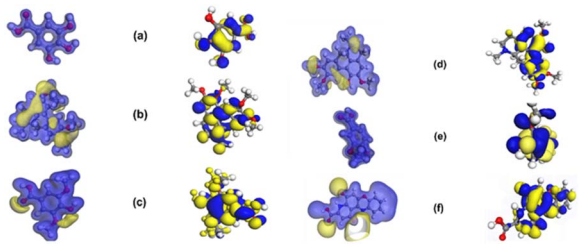

Fig. 12 Single point energy calculation, electron density surface and molecular orbitals of (a) gallic acid (b) glaucine (c) syringic acid (d) thaliporphine (e) vanillic acid (f) catalin.

adopted theoretical method in materials science, DFT offers significant insights into the electronic structure and chemical reactivity of compounds, enabling predictions regarding their performance as corrosion inhibitors.[70] The spatial distribution of reactive sites and the electronic properties that govern the adsorption of the studied molecules on the MS surface were thoroughly investigated through the electrostatic potential (ESP) and frontier molecular orbital (HOMO–LUMO) analyses (Fig. 12), which were conducted using Material Studio.

The ESP mapping revealed distinct regions of high electron density (deep blue to purple), which were primarily concentrated around hydroxyl (–OH), carboxyl (–COOH), and methoxy ($-OCH_3$) groups, as well as over the π-electron clouds of aromatic rings. These electron-rich domains, which are notably evident in gallic, syringic, and vanillic acids, function as robust nucleophilic centers that can donate electron density to the vacant 3d orbitals of surface iron atoms, thereby facilitating chemisorption through coordinate bonding. In contrast, the electron-deficient zones (yellow) that were observed are electrophilic sites that may facilitate the back-donation of electrons from the metal surface into the inhibitor's antibonding orbitals, thereby reinforcing the adsorption process. Although its adsorption footprint is more localized, glaucine still possesses polar functional groups and a polycyclic backbone that enable π–d interactions, hydrogen bonding, and coordinate interactions, despite its reduced size and structural simplicity. Thaliporphine is distinguished by its polyaromatic backbone and extended conjugation, which promote strong π–d orbital overlap and multi-point adsorption, thereby contributing to its high binding stability.

Frontier molecular orbital analysis reinforces these findings by quantitatively assessing electron transfer tendencies. Catalin exhibits the lowest energy gap ($\Delta E = 0.04296$ eV), a hallmark of high electronic polarizability and rapid charge transfer capability, which makes it exceptionally reactive toward the steel surface.[71] Thaliporphine presents the highest HOMO energy (−0.169643 eV), indicating superior electron-donating power and strong affinity for vacant metal orbitals.[72] Phenolic acids such as gallic ($\Delta E = 0.125207$ eV), syringic ($\Delta E = 0.117480$ eV), and vanillic ($\Delta E = 0.132808$ eV) possess moderate ΔE values but benefit from multiple oxygenated functional groups and extended aromatic systems, enabling them to form dense, stable adsorption layers through both chemisorption and physisorption mechanisms. Glaucine ($\Delta E = 0.116386$ eV) has a comparable reactivity to thaliporphine but plays a supplementary role by targeting sites inaccessible to bulkier molecules. The remarkable inhibition efficiency observed experimentally for the molecular mixture arises from a pronounced synergistic effect between these compounds. Catalin and thaliporphine act as primary anchors, initiating strong interactions due to their high softness (low ΔE) and efficient electron donation/acceptance balance. Around these anchoring points, phenolic acids assemble into extended adsorption networks *via* π–d interactions and multiple coordination bonds, effectively increasing surface coverage and reducing defect density in the protective film. Glaucine, owing to its favorable polarity and orbital characteristics, infiltrates residual micro-pores or gaps, interacting with remaining active sites and further blocking corrosive agents such as Cl^- and H^+. This multi-scale cooperative adsorption not only maximizes the coverage of the steel surface but also enhances the mechanical integrity and electrochemical stability of the inhibitor layer, thereby suppressing both anodic dissolution and cathodic hydrogen evolution reactions. To complement this qualitative interpretation, quantitative electronic descriptors—namely the energy gap ($\Delta E = |E\_LUMO - E\_HOMO|$), electronic hardness ($\eta = \Delta E/2$), and molecular softness ($S = 1/\eta$)—were calculated. These parameters are critical in correlating molecular electronic structure with inhibition performance: a small ΔE reflects high reactivity and adaptability to electron exchange, low hardness indicates greater ease of polarization, and high softness enhances adsorption kinetics. The calculated values for each molecule are presented in Table 7, providing a rigorous theoretical framework to explain and predict their corrosion inhibition behavior.

Table 7 Calculated electronic parameters (HOMO, LUMO, ΔE, hardness η, and softness S) of the main molecules

Molecule	E_{HOMO} (eV)	E_{LUMO} (eV)	ΔE (eV)	η (eV)	S (eV^{-1})
Catalin	−0.190123	−0.147163	0.042960	0.021480	46.534
Thaliporphine	−0.169643	−0.136055	0.033588	0.016794	59.529
Gallic acid	−0.210901	−0.085694	0.125207	0.062603	15.972
Syringic acid	−0.207916	−0.090436	0.117480	0.058740	17.026
Vanillic acid	−0.210471	−0.077663	0.132808	0.066404	15.060
Glaucine	−0.183320	−0.066934	0.116386	0.058193	17.184

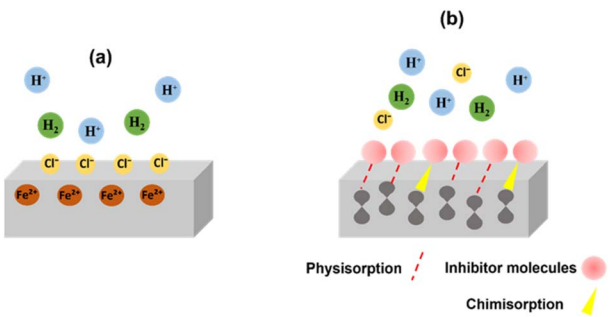

Fig. 13 Illustration of the corrosion process of MS in 1 M HCl (a) in the absence of the inhibitor (b) in the presence of the combined AC–QR extract as a green corrosion inhibitor.

Table 8 Evaluation of inhibitory efficiency of numerous sustainable synergistic inhibitors for MS corrosion in the corrosive solution

Synergistic inhibitors	Corrosive solution	Conc.	Max. EI%	References
Quinoa seed + oestrus ovis larvae	1 M HCl	1 g L^{-1}	86%	76
Lycoris radiata + lycoris chinensis	HF/HCl	—	91.5%	77
Mixture extract of date seeds	1 M HCl	2 g L^{-1}	94.16%	37
Banana peel + rice straw	1 M HCl	750 ppm	96.36%	78
Maple leaves + KI	0.5 M H_2SO_4	200 mg per L MLE + 200 mg per L KI	93.4%	79
Anemone coronaria + *Quercus robur*	1 M HCl	0.5 g L^{-1}	95%	Present work

3.7. Proposed adsorption mechanism

Through comprehensive electrochemical analyses, surface characterization, adsorption studies and quantum chemical calculations, it has been established that the combined extract of *Quercus robur* and *Anemone coronaria* exhibits superior inhibition performance MS corrosion in 1 M HCl solution. This synergistic mixture provides remarkable protection at all tested concentrations, forming a dense and stable adsorption layer at the metal/solution interface, as evidenced by SEM observations showing a smooth, defect-free surface compared to the severely corroded blank specimen. The outstanding inhibition efficiency is attributed to the rich diversity of bioactive compounds present in the extracts, including polyphenolic acids (gallic, syringic, vanillic), alkaloid derivatives (thaliporphine), and small polar molecules. These constituents contain multiple electron-donating functional groups (–OH, –COOH, $–OCH_3$), aromatic π-systems, and heteroatoms, which significantly enhance their ability to adsorb on the steel surface through a mixed mechanism of physisorption and chemisorption. In acidic media, steel dissolution occurs *via* anodic Fe oxidation to Fe^{2+}, while Cl^- ions strongly adsorb on the surface and H^+ ions participate in cathodic hydrogen evolution (Fig. 13(a)).[73] When the inhibitor mixture is introduced, its molecules become protonated due to the acidic environment,[74] allowing electrostatic attraction to the negatively charged metal sites and creating an initial protective layer. Subsequently, chemisorptive interactions occur: oxygen atoms from –OH and –COOH donate lone-pair electrons to vacant Fe orbitals, forming Fe–O coordination bonds, while π-electrons from aromatic rings establish π–d interactions, reinforcing the adsorption layer.[75] ESP mapping and frontier orbital analysis confirm that electron-rich regions localized around these functional groups serve as active sites for interaction, while molecules with high HOMO energy and low ΔE (catalin, thaliporphine) act as primary anchors, initiating strong surface bonding. Phenolic acids further enhance surface coverage by forming multi-point coordination, and small polar molecules such as glaucine infiltrate residual pores, sealing defects. This multi-scale cooperative adsorption leads to the formation of a compact film that hinders Cl^- penetration and blocks both anodic and cathodic reactions (Fig. 13(b)). Thermodynamic parameters support this mechanism: the negative ΔG°_{ads} (-21.34 KJ mol^{-1}) indicates a spontaneous adsorption process involving predominantly physical adsorption with a minor chemisorptive contribution, while the increased activation energy (from 26.23 to 57.73 KJ mol^{-1}) confirms that the barrier effect significantly slows down charge and mass transfer. Consequently, the synergistic action of the extract components provides exceptional protection by reducing metal dissolution and suppressing hydrogen evolution, ensuring the durability of MS in aggressive acidic environments. Table 8 presents a comparison of various sustainable synergistic inhibitors for MS corrosion in an acidic medium, highlighting the remarkable performance of our inhibitor, which achieved 95% inhibition efficiency at an optimal concentration of 0.5 g L^{-1}. This result confirms the potential of *Anemone coronaria* + *Quercus robur* extract as an effective green inhibitor.

4. Conclusion

The corrosion inhibition performance of *Anemone coronaria* (AC) and *Quercus robur* (QR) leaf extracts for mild steel in 1 M HCl was systematically evaluated. Individual extracts achieved high efficiencies (AC: 93.66%, QR: 92%), while their combination reached 95%, indicating a synergistic effect. Compared to previously reported plant extracts, the AC–QR mixture shows superior inhibition, highlighting the benefit of combining extracts with complementary phytochemicals. FT-IR analysis revealed the presence of functional groups responsible for adsorption, and SEM observations showed the formation of a compact protective layer on the steel surface. Adsorption studies indicated that the process follows the Langmuir isotherm and occurs spontaneously, involving a mixed physisorption and chemisorption mechanism. DFT calculations supported these results, revealing strong interactions and high reactivity of inhibitor molecules with the steel surface. The novel combination of AC and QR extracts provides a sustainable, highly effective approach for corrosion mitigation, highlighting its potential for eco-friendly industrial applications in acidic environments.

Author contributions

This study was conducted with significant contributions from all authors. Sofia Kerouad conceptualized the study, designed and executed the experimental work. El-Gherby Youssef performed the formal analysis, including DFT calculations, contributed to data curation and visualization. Issam Forsal supervised the research. Mohammed Amine Edaala analyzed the data and contributed to interpreting the results. Loubna Kabiri prepared the samples. Mohamed Mbarki and Latifa Bouissane reviewed and edited. All authors have reviewed and approved the final manuscript for submission.

Conflicts of interest

There are no conflicts to declare.

Data availability

All data supporting the findings of this study are available within the article.

References

1 Y. Elkhotfi, I. Forsal, E. M. Rakib and B. Mernari, Evaluation of the inhibitor effect of new class triazole derivatives on the corrosion of ordinary steel in hydrochloric acid solution, *Der Pharma Chemica*, 2016, **8**(15), 160–170.

2 A. R. Shahmoradi, M. Ranjbarghanei, A. A. Javidparvar, L. Guo, E. Berdimurodov and B. Ramezanzadeh, Theoretical and surface/electrochemical investigations of walnut fruit green husk extract as effective inhibitor for mild-steel corrosion in 1M HCl electrolyte, *J. Mol. Liq.*, 2021, **338**, 116550, DOI: **10.1016/j.molliq.2021.116550**.

3 A. Zakeri, E. Bahmani and A. S. R. Aghdam, Plant extracts as sustainable and green corrosion inhibitors for protection of ferrous metals in corrosive media: A mini review, *Corros. Commun.*, 2022, **5**, 25–38, DOI: **10.1016/j.corcom.2022.03.002**.

4 M. A. Chidiebere, V. C. Anadebe and R. C. Barik, Insight into the corrosion resistance of mild steel in an acidic environment in the presence of an organic extract: Experimental and computational approach, *Results Eng.*, 2024, **23**, 102787, DOI: **10.1016/j.rineng.2024.102787**.

5 J. K. Emmanuel, Corrosion protection of mild steel in corrosive media, a shift from synthetic to natural corrosion inhibitors: a review, *Bull. Natl. Res. Cent.*, 2024, **48**, 26, DOI: **10.1186/s42269-024-01181-7**.

6 T. D. Manh, T. L. Huynh, B. V. Thi, S. Lee, J. Yi and N. N. Dang, Corrosion Inhibition of Mild Steel in Hydrochloric Acid Environments Containing Sonneratia caseolaris Leaf Extract, *ACS Omega*, 2022, **10**(7), 8874–8886, DOI: **10.1021/acsomega.1c07237**.

7 A. errissoul, A. Ouarhach, F. Benhiba, A. Romane, A. Zarrouk, A. Guenbour, B. Dikici and A. Dafali, Evaluation of Lavandula mairei extract as green inhibitor for mild steel corrosion in 1 M HCl solution: Experimental and theoretical approach, *J. Mol. Liq.*, 2020, **313**, 113493, DOI: **10.1016/j.molliq.2020.113493**.

8 M. Ramezanzadeh, G. Bahlakeh, B. Ramezanzadeh and Z. Sanaei, Adsorption mechanism and synergistic corrosion-inhibiting effect between the green Nettle leaves extract and Zn2+ cations on carbon steel, *J. Ind. Eng. Chem.*, 2019, **77**, 323–343, DOI: **10.1016/j.jiec.2019.04.056**.

9 L. W. El Khatiba, H. T. Rahala and A. M. Abdel-Gaber, Synergistic Effect between Fragaria ananassa and Cucurbita pepo L Leaf Extracts on Mild Steel Corrosio in Hydrochloric Acid Solutions, *Prot. Met. Phys. Chem. Surf.*, 2020, **56**(5), 1096–1106, DOI: **10.1134/S2070205120050111**.

10 R. S. Al-Moghrabi, A. M. Abdel-Gaber and H. T. Rahal, A comparative study on the inhibitive effect of Crataegus oxyacantha and Prunus avium plant leaf extracts on the corrosion of mild steel in hydrochloric acid solution, *Int. J. Ind. Chem.*, 2023, **9**(3), 255–263, DOI: **10.1007/s40090-018-0154-3**.

11 A. Lame, M. Farruku, E. Kokalari, K. Xhanari, N. Isak, K. Xhaxhiu and A. Shehu, Walnut (Juglans regiaL.) fruit septum alcoholic extract as cor-rosion inhibitor for Fe B500B steel bars in mixed acidic solution, *J. Electrochem. Sci. Eng.*, 2024, **14**(3), 297–320, DOI: **10.5599/jese.2303**.

12 S. Abdelaziz, M. Benamira, L. Messaadia, Y. Boughoues, H. Lahmar and A. Boudjerda, Green corrosion inhibition of mild steel in HCl medium using leaves extract of Arbutus unedo L. plant: An experimental and computational approach, *Colloids Surf., A*, 2021, **6**, 126496, DOI: **10.1016/j.colsurfa.2021.126496**.

13 Y. Elkhotfi, I. Forsal, E. M. Rakib and B. Mernari, The inhibition action of essential oil of Juniperus phoenicea on the corrosion of mild steel in acidic media, *Port. Electrochim. Acta*, 2018, **36**(2), 77–87, DOI: **10.4152/pea.201802077**.

14 H. Boubekraoui, I. Forsal, H. Ouradi, Y. Elkhotfi and H. Hanin, Effect of dates extracts as environmentally friendly corrosion inhibitor for carbon steel in 1M HCl solution, *Anal. Bioanal. Electrochem.*, 2020, **12**(6), 828–840.

15 S. Lahmady, O. Anor, I. Forsal, H. Hanine and K. Benbouya, Electrochemical Examination of an Eco-friendly Corrosion Inhibitor, *Anal. Bioanal. Electrochem.*, 2022, **14**(3), 303–318.

16 Q. Wang, X. Zhou, X. Sun, R. Aslam, R. Wang, Y. Sun, Z. Yan and X. Li, Corrosion of Reinforcement in Reinforced Concrete: Influencing Factors, Detection Methods, and Control Techniques—A Review, *J. Test. Eval.*, 2024, **52**(5), 3096–3122, DOI: **10.1520/JTE20230752**.

17 V. Vorobyova, M. Skiba and E. Gnatko, Agri-food wastes extract as sustainable-green inhibitors corrosion of steel in sodium chloride solution: A close look at the mechanism of inhibiting action, *S. Afr. J. Chem. Eng.*, 2023, **43**(1), 273–295, DOI: **10.1016/j.sajce.2022.11.004**.

18 M. Abdallah, K. A. Soliman, B. A. Al Jahdaly, J. H. Al-Fahemi, H. Hawsawi, H. Altass, M. S. Motawea and S. S. Al-Juaid, Natural parsley oil as a green and safe inhibitor for corrosion of X80 carbon steel in 0.5 M H2SO4 solution: a chemical, electrochemical, DFT and MC simulation approach, *RSC Adv.*, 2022, **12**(5), 2959–2971, DOI: **10.1039/D1RA08855F**.

19 H. Boubekraoui, I. Forsal, M. Ellait, K. Benbouya and H. Hanin, Essential Oil of Lavandula intermedia Walberton's Silver Edge as Green Corrosion Inhibitor for Carbon Steel in 1 M HCl Solution, *Anal. Bioanal. Electrochem.*, 2021, **13**(1), 80–93.

20 Y. Fernine, R. Salim, N. Arrousse, R. Haldhar, F. El Hajjaji, S. C. Kim, M. Ebn Touhami and M. Taleb, Anti-corrosion performance of Ocimum basilicum seed extract as environmental friendly inhibitors for mild steel in HCl solution: Evaluations of electrochemical, EDX, DFT and

Monte Carlo, *J. Mol. Liq.*, 2022, **355**, 118867, DOI: 10.1016/j.molliq.2022.118867.

21 W. Emori, R. H. Zhang, P. C. Okafor, X. W. Zheng, T. He and K. Wei, Adsorption and corrosion inhibition performance of multi-phytoconstituents from Dioscorea septemloba on carbon steel in acidic media: characterization, experimental and theoretical studies, *Colloids Surf., A*, 2020, **590**, 124534, DOI: 10.1016/j.colsurfa.2020.124534.

22 A. M. Abdel-Gaber, H. T. Rahal and F. T. Beqai, Eucalyptus leaf extract as a eco-friendly corrosion inhibitor for mild steel in sulfuric and phosphoric acid solutions, *Int. J. Ind. Chem.*, 2023, **11**(2), 123–132, DOI: 10.1007/s40090-020-00207-z.

23 A. M. Abdel-Gaber, H. T. Rahal and M. S. El-Rifai, Green Approach towards Corrosion Inhibition in Hydrochloric Acid Solutions, *Biointerface Res. Appl. Chem.*, 2021, **11**(6), 14185–14195, DOI: 10.33263/BRIAC116.1418514195.

24 R. S. Al-Moghrabia, A. M. Abdel-Gabera and H. T. Rahala, Corrosion Inhibition of Mild Steel in Hydrochloric and Nitric Acid Solutions Using Willow Leaf Extract, *Prot. Met. Phys. Chem. Surf.*, 2019, **55**(3), 603–607, DOI: 10.1134/S2070205119030031.

25 D. C. Hao, X. Gu and P. Xiao, Anemone medicinal plants: ethnopharmacology, phytochemistry and biology, *Acta Pharm. Sin. B*, 2017, **7**(2), 146–158, DOI: 10.1016/j.apsb.2016.12.001.

26 H. O. Elansary, A. Szopa, P. Kubica, H. Ekiert, M. A. Mattar, M. A. Al-Yafrasi, D. O. El-Ansary, T. K. Zin El-Abedin and K. Yessoufou, Polyphenol Profile and Pharmaceutical Potential of Quercus spp. Bark Extracts, *Plants*, 2019, **8**(11), 486, DOI: 10.3390/plants8110486.

27 K. Raafat and A. El-Lakany, Phytochemical and Antinociceptive Investigations of Anemone coronaria Active Part Ameliorating Diabetic Neuropathy Pain, *Planta Medica International Open*, 2018, **5**, e5–e13, DOI: 10.1055/s-0044-100148.

28 E. Burlacu, A. Nisca and C. Tanase, A Comprehensive Review of Phytochemistry and Biological Activities of Quercus Species, *Forests*, 2020, **11**, 0904, DOI: 10.3390/f11090904.

29 *Materials Studio simulation environment, Release 2023*, 2023.

30 J. P. Perdew, K. Burke and M. Ernzerhof, Generalized Gradient Approximation Made Simple, *Phys. Rev. Lett.*, 1996, **77**, 3865, DOI: 10.1103/PhysRevLett.77.3865.

31 B. Aziz, M. Hrimla, M. R. Laamari, I. Elazhary, H. Ben El Ayouchia, M. El Haddad, H. Anane and S. E. Stiriba, Understanding the Corrosion Inhibition Mechanism of Mild Steel in Hydrochloric Acid by a Triazole Derivative: A Combined Experimental and Theoretical Approach, *Prot. Met. Phys. Chem. Surf.*, 2019, **55**, 973–985, DOI: 10.1134/S2070205119050046/METRICS.

32 O. E. Oyeneyin, A. Ibrahim, N. Ipinloju, A. J. Ademoyegun and N. D. Ojo, Insight into the corrosion inhibiting potential and anticancer activity of 1-(4-methoxyphenyl)-5-methyl-N′-(2-oxoindolin-3-ylidene)-1H-1,2,3-triazole-4-carbohydrazide via computational approaches, *J. Biomol. Struct. Dyn.*, 2024, **42**, 11149–11166, DOI: 10.1080/07391102.2023.2260491.

33 J. P. Jaison and J. K. Sebastian, Photocatalytic and antioxidant potential of silver nanoparticles biosynthesized, *Water Pract. Technol.*, 2023, **18**(11), 2664, DOI: 10.2166/wpt.2023.176.

34 R. Idouhli, Y. Koumya, M. Khadiri, A. Aityoub, A. Abouelfida and A. Benyaich, Inhibitory effect of Senecio anteuphorbium as green corrosion inhibitor for S300 steel, *Int. J. Ind. Chem.*, 2019, **10**, 133–143, DOI: 10.1007/s40090-019-0179-2.

35 M. A. Siddiquee, M. U. Parray, M. R. Kamli, M. A. Malik, S. H. Mehdi, K. Imtiyaz, M. Moshahid Alam Rizvi, H. Kumar Rajor and R. Patel, Biogenic synthesis, in-vitro cytotoxicity, esterase activity and interaction studies of copper oxide nanoparticles with lysozyme, *J. Mater. Res. Technol.*, 2021, **13**, 2066–2077, DOI: 10.1016/j.jmrt.2021.05.078.

36 L. Feng, S. Zhang, Y. Qiang, Y. Xu, L. Guo and L. H. Madkour, Experimental and theoretical investigation of thiazolyl blue as a corrosion inhibitor for copper in neutral sodium chloride solution, *Materials*, 2018, **11**(6), 1042, DOI: 10.3390/ma11061042.

37 O. Anor, S. Lahmady, I. Forsal, H. Hanin, H. Ourradi and A. Elharami, An Experimental Investigation of a Date Seeds Hydro-acetonic Mixture Extract Inhibitor for Corrosion Inhibition of Carbon Steel in an Acidic Medium at High Temperatures, *Biointerface Res. Appl. Chem.*, 2023, **13**(3), 271, DOI: 10.33263/BRIAC133.271.

38 A. H. Mostafatabar, G. Bahlakeh, B. Ramezanzadeh, A. Dehghani and M. Ramezanzadeh, A comprehensive electronic-scale DFT modeling, atomic-level MC/MD simulation, and electrochemical/surface exploration of active nature-inspired phytochemicals based on Heracleum persicum seeds phytoextract for effective retardation of the acidic-induced corrosion of mild steel, *J. Mol. Liq.*, 2021, **331**, 115764, DOI: 10.1016/j.molliq.2021.115764.

39 N. Arrousse, Y. Fernine, N. Al-Zaqri, A. Boshaala, E. Ech-Chihbi and R. Salim, Thiophene derivatives as corrosion inhibitors for 2024-T3 aluminum alloy in hydrochloric acid medium, *RSC Adv.*, 2022, **12**(17), 10321–10335, DOI: 10.1039/D2RA00185C.

40 A. Talfana, I. Forsal and S. Lahmady, Inhibition of copper corrosion by Solanum elaeagnifolium extract in 0.5 M H_2SO_4 solution, *Anal. Bioanal. Electrochem.*, 2024, **16**(7), 683–699, DOI: 10.22034/abec.2024.714696.

41 S. Kerouad, I. Forsal and S. Lahmady, Calamintha nepeta extract as an inhibitor of carbon steel corrosion in acidic medium (1 M HCl), *Curr. Top. Electrochem.*, 2023, **24**, 123–131.

42 X. Ren, W. He, J. Liu, Y. Liu and S. Zhou, Corrosion inhibition of imidazoline group on Q235 steel in ethanol gasoline blends: Experimental and computational studies, *J. Mol.*, 2025, **435**, 128166, DOI: 10.1016/j.molliq.2025.128166.

43 A. Thakur, O. Dagdag, A. Berisha, E. E. Ebenso, A. Kumar, S. Sharma, R. Ganjoo and H. Assad, Mechanistic insights into the corrosion inhibition of mild steel by eco-benign Asphodelus Tenuifolius aerial extract in acidic environment: Electrochemical and computational analysis,

Surf. Coat. Technol., 2024, **480**, 130568, DOI: 10.1016/j.surfcoat.2024.130568.

44 A. Talfana, S. Kerouad, I. Forsal, W. Kotmani, L. Kabiri, A. ElHarami and M. Ghazoui, Natural Corrosion Inhibitor from Cistanche Tubulosa Extract for Carbon Steel in HCl: Gravimetric and Electrochemical Characterization, *Prog. Color, Color. Coat.*, 2026, **19**(1), 67–82, DOI: 10.30509/pccc.2025.167509.1383.

45 A. Fouda, S. Etaiw, M. A. Ismail, D. M. El-Aziz and M. Eladl, Novel naphthybithiophene derivatives as corrosion inhibitors for carbon steel in 1 M HCl: Electrochemical, surface characterization and computational approaches, *J. Mol. Liq.*, 2022, **367**(A), 120394, DOI: 10.1016/j.molliq.2022.120394.

46 H. A. Al-sharabi, F. Bouhlal, K. Bouiti, M. Bensemlali, N. Labjar and G. Benabdellah, Study of the corrosion inhibition of C38 steel in a 1M HCl medium by the ethanolic extract of Rumex Nervosus Vahl leaves, *Eur. Phys. J.:Appl. Phys.*, 2022, **97**, 76, DOI: 10.1051/epjap/2022220130.

47 H. T. Rahal, A. M. Abdel-Gaber, R. Awad and B. A. Abdel-Naby, *Anti-Corros. Methods Mater.*, 2018, **65**, 430–435.

48 H. T. Rahal, A. M. Abdel-Gaber and R. Awad, *Chem. Eng. Commun.*, 2017, **204**, 348–355.

49 S. Abdoune, N. Aliouane, A. Hellal, M. Al-Noaimi, N. Sait, N. Chafai, L. Toukal and N. A. Ahmed, Two α-aminophosphonics acids as corrosion inhibitors for carbon steel in 0.5M HCl: Electrochemical and DFT/MD simulation, *J. Mol. Struct.*, 2024, **1295**, 136673, DOI: 10.1016/j.molstruc.2023.136673.

50 M. S. Numin, K. Jumbri, K. E. Kee, A. Hassan, N. Borhan and J. Matmin, DFT Calculation and MD simulation studies on gemini surfactant corrosion inhibitor in acetic acid media, *Polymers*, 2023, **15**(9), 2155, DOI: 10.3390/polym15092155.

51 F. S. de souza and A. Spinelli, Caffeic acid as a green corrosion inhibitor for mild steel, *Corros. Sci.*, 2009, **51**(3), 642–649, DOI: 10.1016/j.corsci.2008.12.013.

52 N. A. N. K. Baharin, S. A. I. Sheikh Mohd Ghazali, S. Syaida Sirat, A. M. Tajuddin, N. Hidayah Pungot, E. Normaya, S. R. M. Kamarudin and N. N. Dzulkifli, In-depth investigation of corrosion inhibition mechanism: Computational, electrochemical, and theoretical studies of vanillin meldrum's acid on mild steel surface in 1 M HCl, *J. Mol. Liq.*, 2024, **416**(B), 126390, DOI: 10.1016/j.molliq.2024.126390.

53 H. Ferkous, A. Sedik, A. D. R. Redjemia, K. abdasalem, C. Boulechfar, A. Abdennouri, A. Madaci, M. Berredjem, A. Boublia, M. S. Ali, B. Jeon, K. K. Yadav and Y. Benguerba, A comparative study of novel synthesized sulfamide compounds: Electrochemical, morphological, XPS, and theoretical investigations on copper corrosion inhibition in 1.0 M HCl, *J. Mol. Liq.*, 2024, **394**, 123781, DOI: 10.1016/j.molliq.2023.123781.

54 F. Bentiss, C. Jama, B. Mernari, H. El Attari, L. El Kadi and M. Lebrini, Corrosion control of mild steel using 3, 5-bis (4-methoxyphenyl)-4-amino-1, 2, 4-triazole in normal hydrochloric acid medium, *Corros. Sci.*, 2009, **51**(8), 1628–1635, DOI: 10.1016/j.corsci.2009.04.009.

55 F. Mohammadinejad, S. M. A. Hosseini, M. S. Zandi, M. J. Bahrami and Z. Golshani, Metoprolol: new and efficient corrosion inhibitor for mild steel in hydrochloric and sulfuric acid solutions, *Acta Chim. Slov.*, 2020, **67**, 710–719, DOI: 10.17344/acsi.2019.5301.

56 H. A. El Nagy, E. H. El Tamany, H. Ashour, O. E. El-Azabawy, E. G. Zaki and S. M. Elsaeed, Polymeric ionic liquids based on Benzimidazole derivatives as corrosion inhibitors for X-65 carbon steel deterioration in acidic aqueous medium: hydrogen evolution and adsorption studies, *ACS Omega*, 2020, **5**, 30577–30586, DOI: 10.1021/acsomega.0c04505.

57 S. Cherrad, A. A. Alrashdi, H. S. Lee, H. Lgaz, B. Satrani and M. Ghanmi, Cupressus arizonica fruit essential oil: A novel green inhibitor for acid corrosion of carbon steel, *Arabian J. Chem.*, 2022, **15**(6), 103849, DOI: 10.1016/j.arabjc.2022.103849.

58 A. Hattak, S. Izzaouihda, Z. Rouifi, F. Benhiba, S. Tabti and A. Djedouani, Anti-corrosion performance of pyran-2-one derivatives for mild steel in acidic medium: electrochemical and theoretical study, *Chem. Data Collect.*, 2021, **32**, 100655, DOI: 10.1016/j.cdc.2021.100655.

59 S. Echihi, N. Benzbiria, M. E. Belghiti, M. El Fal, M. Boudalia, E. M. Essassi, A. Guenbour, A. Bellaouchou, M. Tabyaoui and M. Azzi, Corrosion inhibition of copper by pyrazole pyrimidine derivative in synthetic seawater: Experimental and theoretical studies, *Mater. Today*, 2020, **37**(3), 3958–3966, DOI: 10.1016/j.matpr.2020.09.264.

60 M. E. Belghiti, Y. El Oudadi, S. Echihi, A. Elmelouky, H. Outada, Y. Karzazi, M. Bakasse, C. Jama, F. Bentiss and A. Dafali, Anticorrosive properties of two 3,5-disubstituted-4-amino-1,2,4-triazole derivatives on copper in hydrochloric acid environment: Ac impedance, thermodynamic and computational investigations, *Surf. Interfaces*, 2020, **21**, 100692, DOI: 10.1016/j.surfin.2020.100692.

61 M. R. Gholamhosseinzadeh, H. Aghaie, M. Shahidi Zandi and M. Giahi, Rosuvastatin drug as a green and effective inhibitor for corrosion of mild steel in HCl and H2SO4 solutions, *J. Mater. Res. Technol.*, 2019, **8**(6), 5314–5324, DOI: 10.1016/j.jmrt.2019.08.052.

62 N. Benzbiria, S. Echihi, M. E. Belghiti, A. Thoume, A. Elmakssoudi, A. Zarrouk, M. Zertoubi and M. Azzi, Novel synthetized benzodiazepine as efficient corrosion inhibitor for copper in 3.5% NaCl solution, *Mater. Today*, 2020, **37**(3), 3932–3939, DOI: 10.1016/j.matpr.2020.09.030.

63 M. E. Belghiti, M. Mihit, A. Mahsoune, A. Elmelouky, R. Mghaiouini, A. Barhoumi, A. Dafali, M. Bakasse, M. A. El Mhammedi and M. Abdennouri, Studies of inhibition effect 'E & Z' configurations of hydrazine derivatives on mild steel surface in phosphoiric acid, *J. Mater. Res. Technol.*, 2019, **8**(6), 6336–6353, DOI: 10.1016/j.jmrt.2019.09.051.

64 M. Abdallah, J. H. Al-Fahemi, K. A. Soliman, A. S. Al-Gorair, M. S. Al-Sharif and S. S. Al-Juaid, Exploring cinnamon extract's potential as a green corrosion inhibitor for X65 carbon steel in sulfuric acid: a comprehensive

investigation, *J. Dispersion Sci. Technol.*, 2024, 1–15, DOI: 10.1080/01932691.2024.2333537.

65 F. El-Hajjaji, M. Messali, A. Aljuhani, M. R. Aouad, B. Hammouti, M. E. Belghiti, D. S. Chauhan and M. A. Quraishi, Pyridazinium-based ionic liquids as novel and green corrosion inhibitors of carbon steel in acid medium: Electrochemical and molecular dynamics simulation studies, *J. Mol. Liq.*, 2018, **249**, 997–1008, DOI: 10.1016/j.molliq.2017.11.111.

66 L. Ghalib, H. J. M. Al Jaaf and H. A. Abdulghani, Temperature effect on the efficiency of Eucalyptus Camaldulensis leaves in the acid corrosion of carbon steel, *Mater. Today: Proc.*, 2021, **42**, 2475–2481, DOI: 10.1016/j.cdc.2021.100655.

67 M. Al-Noaimi, S. Benabid, H. Hamani, Q. F. A. Salman, M. Binsabt, F. F. Awwadi, K. Douadi and T. Douadi, Corrosion inhibition of carboxylate substituted amidrazone on mild steel in 3% NaCl medium: Electrochemical, DFT and molecular dynamics simulation studies, *Chem. Data Collect.*, 2022, **40**, 100877, DOI: 10.1016/j.cdc.2022.100877.

68 A. Zaher, R. Aslam, H. S. Lee, A. Khafouri, M. Boufellous, A. A. Alrashdi, Y. El aoufir, H. Lgaz and M. Ouhssine, A combined computational & electrochemical exploration of the Ammi visnaga L. extract as a green corrosion inhibitor for carbon steel in HCl solution, *Arabian J. Chem.*, 2022, **15**, 103573, DOI: 10.1016/j.arabjc.2021.103573.

69 I. Dhouibi, F. Masmoudi, M. Bouaziz and M. Masmoudi, A study of the anti-corrosive effects of essential oils of rosemary and myrtle for copper corrosion in chloride media, *Arabian J. Chem.*, 2021, **14**, 102961, DOI: 10.1016/j.arabjc.2020.102961.

70 L. K. Ojha, B. Tüzün and J. Bhawsar, Experimental and theoretical study of Effect of Allium sativum extracts as corrosion inhibitor on mild steel in 1 M HCl medium, *J. Bio. Tribo. Corros.*, 2020, **6**, 1–10, DOI: 10.1007/s40735-020-00336-z.

71 R. K. Mehta, S. K. Gupta and M. Yadav, Studies on pyrimidine derivative as green corrosion inhibitor in acidic environment: electrochemical and computational approach, *J. Environ. Chem. Eng.*, 2022, **10**, 108499, DOI: 10.1016/j.jece.2022.108499.

72 M. Bozorg, A. Koochakiabkenar and Y. Ashouri, Combined Electrochemical and DFT Approaches to Elaeagnus Angustifolia Extract as a Green Corrosion Inhibitor for Mild Steel in HCl Solution, *J. Mol. Liq.*, 2025, **434**, 127993, DOI: 10.1016/j.molliq.2025.127993.

73 H. Kumar, P. Yadav, R. Kumari, R. Sharma, S. Sharma, D. Singh, H. Dahiya, P. Kumar, S. Bhardwaj and P. Kaur, Highly efficient green corrosion inhibitor for mild steel in sulfuric acid: experimental and DFT approach, *Colloids Surf., A*, 2023, **675**, 132039, DOI: 10.1016/j.colsurfa.2023.132039.

74 M. A. Ahmed, S. Amin and A. A. Mohamed, Current and emerging trends of inorganic, organic and eco-friendly corrosion inhibitors, *RSC Adv.*, 2024, **14**, 31877–31920, DOI: 10.1039/D4RA05662K.

75 N. O. Eddy, U. J. Ibok, R. Garg, R. Garg, A. Iqbal, M. Amin, F. Mustafa, M. Egilmez and A. M. Galal, A brief review on fruit and vegetable extracts as corrosion inhibitors in acidic environments, *Molecules*, 2022, **27**, 2991, DOI: 10.3390/molecules27092991.

76 A. Hafazeh, H. Mobtaker, M. Azadi and M. Rassouli, Theoretical and experimental studies on the electrochemical behavior of steel in HCl solution in the presence of two bio-inhibitor mixtures, *Heliyon*, 2024, **10**(20), e39066, DOI: 10.1016/j.heliyon.2024.e39066.

77 Z. Xia and X. Zhang, Study on Corrosion Resistance of Carbon Steel in HF/HCl Acid Mixture in Presence of Lycoris radiata and Lycoris chinensis Leaf Extract as Environmentally Friendly Corrosion Inhibitor, *Int. J. Electrochem. Sci.*, 2022, **17**, 220921, DOI: 10.20964/2022.09.20.

78 M. Dazdari, A. Khormali and A. Taleghani, Analysis of a Mixture of Banana Peel and Rice Straw Extracts for Inhibiting Corrosion of Carbon Steel in Hydrochloric Acid Solution, *Appl. Sci.*, 2025, **15**(9), 5026, DOI: 10.3390/app15095026.

79 Y. Wang, Y. Qiang, H. Zhi, B. Ran and D. Zhang, Evaluating the synergistic effect of maple leaves extract and iodide ions on corrosion inhibition of Q235 steel in H2SO4 solution, *J. Ind. Eng. Chem.*, 2023, **117**, 422–433, DOI: 10.1016/j.jiec.2022.10.030.